Monochromatised XUV Beamline for ultrafast Time-Resolved ARPES

Contact *Cephise.Cacho@stfc.ac.uk*

E. Springate, C. Cacho, E. Turcu, C. Froud, S. G. Hook
Artemis, Central Laser Facility, Didcot, UK

L. Poletto, P. Villoresi, F. Frassetto, S. Bonora
LUXOR, Padova, Italy

W. Bryan, J. Nemeth
Swansea University, Swansea, UK

A. Cavalleri, J. Petersen, N. Dean
University of Oxford, UK

A. Cavalieri, S. Kaiser
Centre for Free Electron Laser Science , Hamburg, Germany

S. Dhesi
Diamond Light Source , RAL, UK

Introduction

The short pulses of coherent XUV radiation produced through high harmonic generation have enabled the study of ultrafast electron dynamics in atomic systems and simple molecules. The Artemis facility now aims to exploit these XUV pulses to investigate ultrafast dynamics in experiments spanning gas-phase chemistry of polyatomic molecules and condensed-matter physics of complex materials

We have built an XUV beamline that delivers short pulses of monochromatised XUV, produced through high harmonic generation, to an end-station optimized for photo-emission experiments on condensed matter. We have shown that the beamline can achieve 250 meV energy resolution and 30 fs temporal resolution, enabling us to carry out first measurements of time-resolved photoemission with XUV pulses.

The core source of the Artemis facility is a Ti:Sa CPA laser system with two amplifier stages delivering 14 mJ/pulse, 30 fs, 800 nm pulses at 1 kHz repetition rate. The output beam is divided in three branches: 10 mJ allocated to a high power OPA (1 mJ @ 1.3 µm output) to cover the wavelength region 200 nm – 15 µm, 1 mJ for short pulse (7 fs) by hollow fiber compression and the rest for other pump applications. All the beams are Carrier Envelope Phase stabilized and intrinsically synchronized. Any of the beamlines can be used to generate XUV pulses through high harmonic generation, or used as synchronized pump and probe pulses.

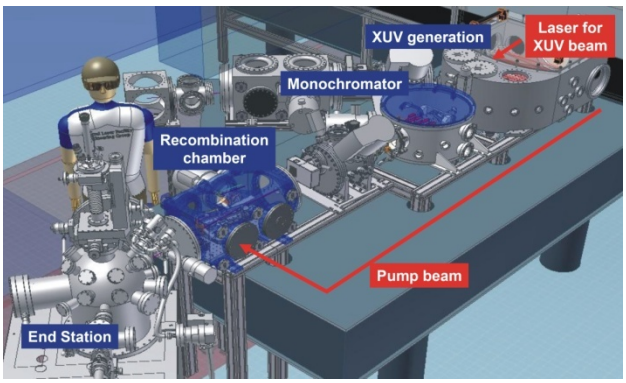

Figure 1: Layout of the XUV beamline including the Harmonic generation chamber, the monochromator chamber to select the photon energy, the recombination chamber for pump-probe experiment and the experimental chamber for time resolved ARPES.

The principal elements of the XUV beamline are the HHG chamber to generate short wavelength pulses, the monochromator to select the photon energy, the recombination chamber to align the pump/probe beams and the End-Station to perform the photoemission experiment (see Figure 1). All the optical elements are mounted on the optical bunch and the vacuum chambers are isolated to minimize the mechanical vibrations.

High Harmonic Generation

High Harmonic Generation is a well established technique to produce short wavelength (12 nm , 100 eV) photons using high peak power tabletop laser sources. In a vacuum chamber, a lens focuses the drive laser beam onto a pulsed (1 kHz) gas jet synchronized with the laser system. After the interaction region the harmonics propagate collinearly to the incident beam with a smaller divergence angle (Figure 2a). During the laser-atom interaction, the Coulomb potential of the atom is deformed by the laser field allowing the tunneling of an outer electron in the vacuum. When the laser field changes polarity the electron is reaccelerated towards the ion. Then the electron recombines with the ion emitting an XUV photon (Figure 2b). For symmetry reasons only odd harmonics are generated.

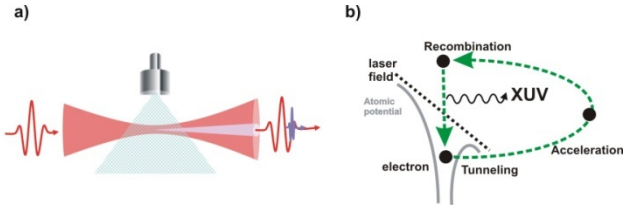

Figure 2: a) Sketch of the harmonic generation process. A pulsed laser with high peak power is focused on a gas jet. The harmonics propagate collinearly to the incident beam with a smaller divergence. b) Three steps model of the High Harmonic Generation: atomic ionization, electron acceleration and electron recombination generating the XUV photon.

The harmonic generation efficiency depends on the phase matching conditions at the interaction region and it is controlled by the drive beam diameter, the focal lens and the pulse energy, as well as gas pressure, length of interaction region and the position of the laser focus relative to the gas-jet. On a daily basis our conditions are 8 mm, 50 cm, 800 microJ respectively and we use 2 bar of Ar in a ~5mm long interaction region. The highest photon energy reachable depends on the gas used (Ar, Ne) and the wavelength (800 nm – 1.3 µm) of the drive beam.

Monochromator

The monochromator was developed in collaboration with LUXOR laboratory [1]. It was designed to select one single harmonic from the spectrum and preserve the harmonic pulse duration (~10fs). A first toroidal mirror collimates the incident beam and deflects it onto a plane diffraction grating. The diffracted light is refocused by a second toroidal mirror on to the exit slit (Figure 3a). The grating is used in conical illumination to limit the time spread of the pulses. Four gratings are mounted on a translation stage to cover the energy range 20-

100eV with resolving powers corresponding to either 10 fs or 50 fs pulse duration.

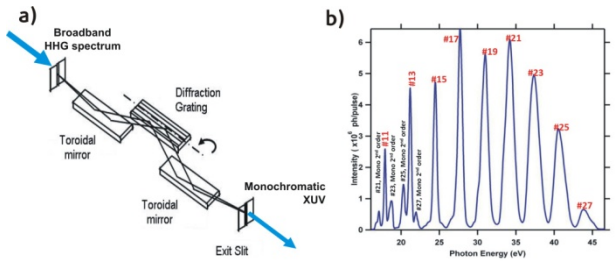

Figure 3: a) Layout of the monochromator including two toroidal mirrors to collimate the XUV on the grating and to refocus the beam on the exit slit after diffraction. b) Example of Ar harmonic yield measured after the exit slit.

The transmitted XUV intensity is measured by inserting a calibrated channeltron in the beam after the exit slit. In Figure 3 we present an example of harmonic yield obtained by rotating the grating and converting the rotation angle into photon energy.

Recombination chamber

After the monochromator exit slit the XUV beam diverges and is reimaged on the sample with a toroidal mirror in the recombination chamber. The gold coated toroidal mirror operates in 2f geometry at grazing incidence (4°). The 5 axis motorized mirror mount allows fine control of the spot size and shape on the sample. The pump beam (200 nm - 15 µm) travels on the side of the beamline and is focused on the sample with a lens mounted on the optical table. In the recombination chamber the XUV beam goes through a holey mirror and the pump beam is reflected at 90° by this mirror to operate in collinear mode. A mirror mounted on a linear drive deflects temporally both beams to find the spatial and temporal overlap at the focal point (in air). The pressure gradient between the recombination chamber and the UHV chamber is maintained by a 2 mm diameter pin hole mounted on an XY translation.

Experimental Chamber

The experimental end-station is a fully equipped UHV chamber with a mu-metal shielding. The sample is mounted on a 5 axis manipulator with He cooling down to 14K. A load-lock allows fast transfer of the sample into the main chamber. After in-situ cleaving the surface quality is controlled with a LEED analyzer. The photoemission is performed with a hemispherical analyzer (PHOIBOS 100) where both angle and energy are resolved simultaneously. The analyzer resolution is better than 25 meV measured on Ag Fermi edge at low temperature. Depending on the electron optics mode, electrons are collected with high angular resolution (±0.1°) or over a large angular dispersion (±13°). A He lamp is available for off line sample characterization.

Energy and Time Resolution

In order to characterize the beamline overall energy resolution we present in Figure 4a the TaS2 Fermi edge measured at room temperature using the monochromatized 17th harmonic. The red curve is a fitting of the data with a Fermi-Dirac function convolved to a 250 meV width Gaussian function. The XUV beam was monochromatized with the highest resolution grating ($E/\Delta E = 100$) and the exit slit set at 100 µm. The photoemission energy resolution achieved (250 meV) is limited by the monochromator resolving power, which is designed to preserve the pulse duration of the ultrafast harmonics (~ 10 fs).

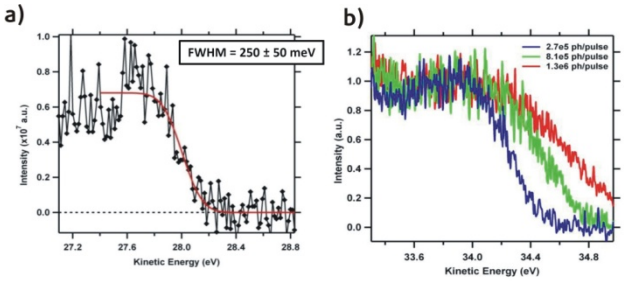

Figure 4: a) Fermi edge measured on TaS_2 with the 17th harmonic of Ar (28 eV). The overall photoemission resolution is 250 meV deduced from the fitting of the edge (red curve). b) Effect of the XUV power on the Fermi edge (broadening and shifting). Above 3.10^5 ph/pulse the space charge effects become non negligible for a 50 µm*50 µm spot size on the sample.

Carrying out photoemission experiments with a 1 kHz pulsed source, one has to be careful to the photon flux due to space charge effects. Indeed if too many electrons are emitted in the vacuum by a single photon pulse, those electrons will interact by Coulomb repulsion in the region very close to the sample surface. Consequently the spectral information (kinetic energy) from the photoemission process will be altered. Figure 4b shows the Fermi edge of TaS_2 measured with the 21st harmonic at three XUV fluxes (normalized at 33.8 eV kinetic energy). The broadening and shift of the edge is a signature of space charge effects and imposes a flux upper limit of ~3.10^5 ph/pulse for a 50µm*50µm spot size on the sample.

The time resolution of the monochromatised XUV beam was determined by measuring the Kr^{2+} ion yield using an ion time-of-flight spectrometer. The Kr atom are pumped with the 23rd harmonic (35.7 eV) producing Kr^+ ion in a long-lived excited state. The 800 nm (1.55 eV) probe beam can then ionize the excited ion to Kr2+ for positive delay time between the pulses. From the sharp step in the Kr^{2+} yield we extract the XUV pulse duration of 24 fs starting with an IR pulse of 28 fs. Further details about this experiment are presented in this year annual report by W. Bryan *et al.* .

Conclusion

The XUV beamline with the photoemission experimental chamber are now available to users. Our first time resolved ARPES measurements are presented in this year annual report by J.C. Petersson *et al.* .

References

1. F Frassetto, S Bonora, P Villoresi, L Poletto, E Springate, CA Froud, ICE Turcu, AJ Langley, DS Wolff, JL Collier, SS Dhesi and A Cavalleri, SPIE Proc. Vol. **7077**, Advances in X-Ray/EUV Optics and Components III, 707713 (2008)

Spin and Angle resolved photoemission with fs laser source: calibration of spin detector

Contact *cephise.cacho@stfc.ac.uk*

C.M. Cacho
Artemis, Central Laser Facility, STFC, Didcot, UK

E.A. Seddon
Department of Physics, Manchester University, UK

C.M. Cacho, S. Vlaic, M. Malvestuto, B. Ressel, and F. Parmigiani
Sincrotrone Trieste, Trieste, Italy

The experiments presented here were carried out at the Sincrotrone Trieste within the frame of FERMI@Elettra free electron laser project through an international collaboration with the CLF/Artemis project. Here a fs-laser source is combined to the Time-of-Flight-Spin electron analyzer developed at STFC-Daresbury for performing spin, angle and time resolved photoemission spectroscopy experiments on solids.

Introduction

Angle resolved photoemission is a very powerful technique to explore the electronic structure of materials in order to understand their macroscopic properties. Over the past three decades this spectroscopic technique has well matured partly due to the development intense synchrotron radiation source and bright fs-laser source. Measuring the spin as well as the emission angle of the photoelectron is particularly interesting to study the magnetic properties of ferromagnetic systems or systems with large spin-orbit coupling [1-2]. The intrinsic low efficiency of the electron spin detection makes these experiments very challenging. This is why, combining very bright photon source (like table top laser source) with novel electron analyzer (electron time-of-flight) is a real step forward for this type of experiments particularly in term of acquisition time and resolution. We have developed an electron time-of-flight (ToF) spin analyzer where all the electrons are spin and energy- resolved simultaneously regardless of their kinetic energy. Essentially a very high efficiency electron detector (ToF) is combined to a spin detector (mini Mott polarimeter).

The spin polarization P of an electron beam is defined by the asymmetry $P = (n^{\uparrow} - n^{\downarrow})/(n^{\uparrow} + n^{\downarrow})$, where $n^{\uparrow(\downarrow)}$ is the number of spin up (down) electron. In order to extract the spin polarization from the experimental data the spin sensitivity of the polarimeter, *i.e.* the Sherman function, must be evaluated. Very few precise spin calibrations have been reported so far in the literature because of the difficulty of producing either an electron beam of well known spin polarization or a fully spin polarized electron beam. However an interesting source of highly polarized electron is the Au(111) Surface States (SS) which are free electrons localized at the metal surface. Enhanced spin-orbit coupling (the Rashba-Bychkov effect) is observed due to the high atomic number of gold. In the following work we are using both SS as reference to perform the calibration of the Mott polarimeter.

Laser system and electron analyser

The laser system used is a regenerative amplifier system (RegA9050 from Coherent) providing photon pulses at a repetition rate of 250 kHz with a pulse energy of 5 µJ and a photon energy of 1.55 eV (800 nm). The 4th harmonic (6.2 eV) of the fundamental beam was obtained by harmonic generation in phase matched BBO crystals. The beam size on the sample was 100µm diameter with 5pJ pulse energy and 160fs pulse duration.

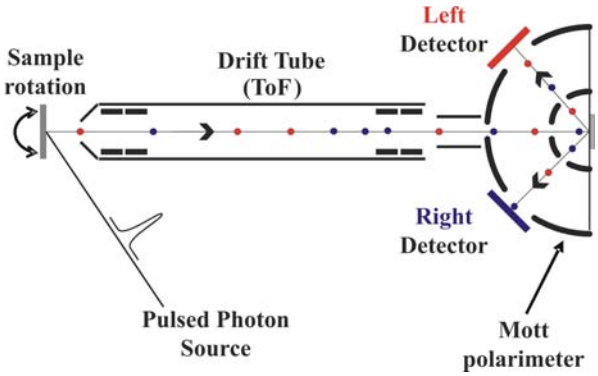

Fig.1 : Top view of the experimental setup in normal emission geometry. The photoelectrons travel through the drift tube up to the Mott polarimeter where they accelerated to 20 kV and the back scattered beam is measured. The arrival time of the electrons at each detector is measured and converted to kinetic energy. The vertical spin polarisation is resolved with the Left-Right detectors of the Mott polarimeter.

In an ultrahigh vacuum (UHV) chamber (10^{-10}mbar) a Au(111) single crystal was mounted on a sample holder with control of the polar (theta, vertical axis) and azimuthal (phi, surface-normal axis) angles. The surface was prepared by Ar ion sputtering and annealing to 400˚C. The reconstruction of the surface was monitored using Low Energy Electron Diffraction.

A sketch of the ToF analyser and Mott polarimeter are presented in Fig.1 . The ToF analyzer is composed of input electron optics, a 25 cm long drift tube and output electron optics which taken together position the Mott polarimeter scattering foil 45 cm from the sample. In the particular case of very low photon energy, all the ToF electrodes are grounded and the electron trajectory in the ToF is considered as ballistic. The angular resolution is then given by the 3 mm diameter entrance hole of the Mott polarimeter and is estimated to be ±0.19deg. All the electrons within this solid angle are accelerated in the Mott polarimeter, hit the targeted gold foil and the back-scattered electrons are measured on four sets of Micro Channel Plate (MCP) detectors. The maximum energy lost in the scattering process is controlled by the Mott polarimater energy window which was set to 500 eV. The electron arrival time is measured on each detector by a Time-to-Digital-Converter (GPTA mbH) with a time

digitization of 120 ps, the arrival time was then converted to kinetic energy. The overall time resolution of the electronics was 293 ps corresponding to an ultimate energy resolution of 2 meV. The energy resolution of the measurements presented here is evaluated at 25 meV limited by the band width of the laser pulse. The vertical spin polarization of the electrons is deduced from the left-right detectors of the polarimeter. A top-bottom detector pair is available for the horizontal spin polarization (not shown in Fig.1).

Determination of the Mott polarimeter spin sensitivity

At normal emission both spin up and down SS have the same binding energy due to the fact that the momentum of the electrons in the initial state is zero. As the sample is rotated electrons with larger parallel momentum are detected and the fully spin polarized SS are splitted. For a sample angle of -12.2° between the surface normal and the ToF acceptance direction, the averaged EDC (Fig.2-a) obtained from the Mott polarimeter four detectors shows a broad structure just below the Fermi edge corresponding to two peaks. At room temperature the thermal broadening is larger than the energy splitting so to determine the positions and the width of the SS we performed a double Voigt function fitting (solid line). A flat background was subtracted in order to remove the unpolarized contribution from the sp-band. On the averaged EDC both SS have similar total intensity whereas the EDCs measured with the Left (Fig.2-b) and Right (Fig.2-c) detectors show different ratios according to the spin polarization of the photoelectrons.

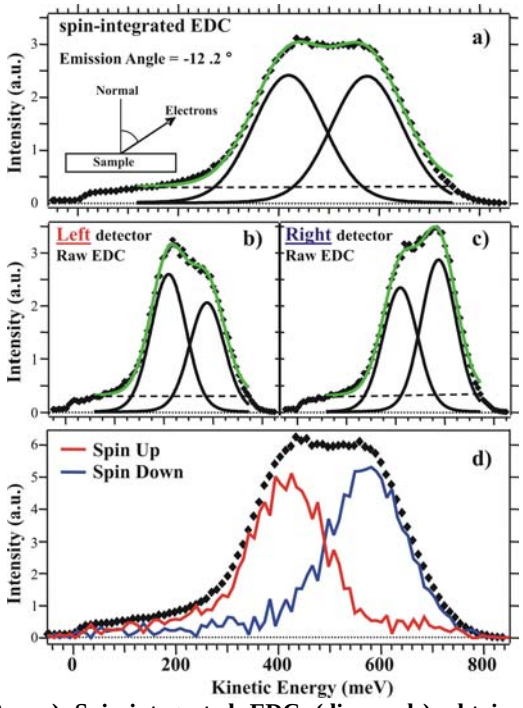

Fig.2 : a) Spin-integrated EDC (diamonds) obtained by averaging the four detectors of the Mott polarimeter. The surface states energy positions and widths are extracted using a double Voigt fitting function (black curves) assuming a flat background. b)c) Left-Right detector EDC fitted with the parameters from a). Only the amplitude of the surface states is left as a free parameter. d) Spin-resolved EDC (red and blue curves) obtained from the EDC spectra of panel b) and c).

The four total intensities of the SS measured in Left-Right detectors are deduced from the Voigt fitting of the raw EDCs Fig.2-b-c. Using a symmetric relation between those quantities one can extract the experimental asymmetry and the effective Sherman function of the Mott polarimeter. In the present case we obtained $A_{\exp} = 2.6 \pm 0.2\%$ and $S_{eff} = 10.8 \pm 0.7\%$ for an accelerating voltage of 20kV in the Mott polarimeter. Finally the spin-resolved EDC (Fig.2-d) are calculated with the relation $I_{\uparrow(\downarrow)}(E) = I(E).(1 \pm P(E))$ where $I(E)$ is the average spin integrated spectrum (Fig.2-a). Fig.2-d shows that both SS are clearly resolved with a constant sp-band background. With a photoelectron trajectory calculation we obtain a real emission angle of 19.1° (20.2°) for SS1 (SS2) of Fig.2-d which correspond to the momentum $\mathbf{k}_{SS1}$ = 0.126 Å^{-1} ($\mathbf{k}_{SS2}$ = 0.114 Å^{-1}). Those results are in very good agreement with ARPES measurements performed at higher photon energy [3].

Variation of the Mott polarimeter high voltage

The scattering efficiency of the Mott polarimeter is defined by the ratio I / I_0 where I is the current measured in the detectors and I_0 is the current injected in the polarimeter. The spin efficiency of the Mott polarimeter depends strongly on the accelerating voltage V_{Mott} applied on the target gold foil.

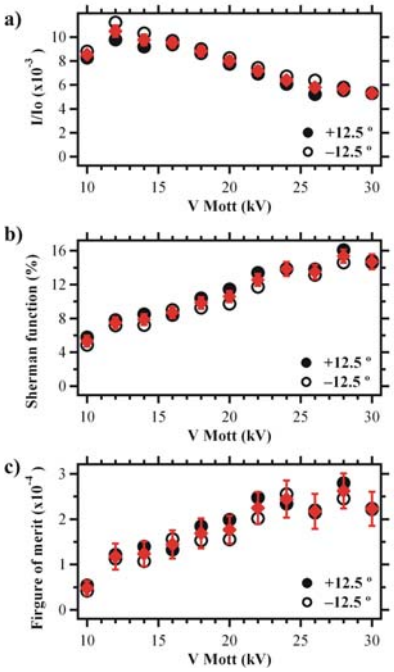

Fig.3 : a) The scattering efficiency I/Io decreases with the Mott polarimeter high voltage. The measurements were performed at +12.5° (circle) and -12.5° (solid circle) from normal emission. Red diamonds are the average intensity. b) The value of the spin selectivity of the Mott polarimeter (Sherman function) increases up to 15% with the accelerating voltage. c) As the Mott high voltage increases, the Figure of merit increases to reach a plateau at 25kV.

In Fig.3 we present the variation of both the ratio I / I_0 (Fig.3-a circles) and the S_{eff} (Fig.3-b circles) measured in two photoemission directions (±12.5° from the surface normal) and for various V_{Mott} values between 10kV and 30kV. The average values are deduced (Fig.3 diamonds) and the error bars are calculated from the fitting parameter errors for a confidence interval of 95%. The dispersion of the measurements for both sample angles is within the error bars. In the voltage region 20-30 kV the effective Sherman function is measured with an

overall error of ±6% which is consistent with the best results reported in the literature. Thus setting our apparatus as a reliable and high performance system for spin-resolved ARPES. Between 10-30 kV accelerating potential the scattered intensity decreases by ~50% whereas the Sherman function increases by ~300%. This large increase of the Sherman function is consistent with the increase in the gradient of Coulomb potential (and so the spin-orbit interaction) as the incident electrons travel closer to the Au nucleus.

Assuming a merely statistical error for the measurements ($\Delta I = \sqrt{I}$) the spin polarization error is $\Delta P = 1/\sqrt{IS^2}$ where IS^2 is the figure of merit (FOM) of the Mott polarimeter. Fig.3-c shows the FOM calculated from the results of Fig.3-a-b. The FOM increases with V_{Mott} to reach a plateau at ~25 kV, the optimal voltage to operate the ToF-Spin analyzer.

Conclusion

We have performed spin and angle-resolved photoemission on Au(111) at very low photon energy. The good efficiency of the electron ToF-Spin analyser allowed us to work with high angular and energy resolution while still maintaining a short acquisition time (~ 10 min). The spin-orbit coupling of the SS was spin-resolved and analysed as a fully spin polarized electron source. The effective spin sensitivity of the Mott polarimeter was extracted from the raw measurements for various Mott voltages up to 30kV. The figure of merit shows that the optimal condition to operate the Mott polarimeter is ~25 kV [4].

1 J.-H. Park *et al.*, Nature, **392**, 794 (1998).
2 K. Sakamoto *et al*., Phys. Rev. Lett., **102**, 096805 (2009)
3 M. Hoesch *et al.*, Phys. Rev. B 69, 241401 (2004).
4 C.M. Cacho *et al.*, Rev. Sci. Instrum. **80**, 043904 (2009)

Few-cycle carrier-envelope-phase controlled laser pulses for time resolved science at the Artemis facility

Contact *emma.springate@stfc.ac.uk*

W. A. Bryan, G.R.A.J. Nemeth

Department of Physics, Swansea University and Central Laser Facility, STFC Rutherford Appleton Laboratory

R. B. King

School of Mathematics and Physics, Queen's University Belfast

C. M. Cacho, I. C. E. Turcu and E. Springate

Central Laser Facility, STFC Rutherford Appleton Laboratory

Introduction

When the duration of a laser pulse reaches the few-cycle level, the phase of the laser electric field relative to the pulse envelope (the carrier-envelope phase, CEP) can have a significant effect on the physics of the interaction. Examples of this are the generation of isolated attosecond pulses [1] and the control of electron localisation during molecular dissociation [2], both of which require few-cycle pulses with stable carrier-envelope phase.

The Artemis facility [3, 4] for ultrafast XUV science is constructed around a high power CEP stabilised laser system with an output of 780 nm, 30 fs, 14mJ/pulse, 1kHz. Part of the energy can be split off to generate few-cycle CEP-stabilised pulses at 780nm and tuneable pulses from the UV to the mid-IR. These can be flexibly configured to produce femtosecond XUV pulses through high harmonic generation (HHG), or used as pump and probe pulses. We have recently made improvements to the few-cycle beamline to reduce the pulselength to 7 fs and measured the long-term performance of the CEP stabilisation.

Carrier-envelope phase control

The laser is CEP stabilised using commercial f-to-2f interferometers to measure the CEP drift and feedback electronics. A fast CEP loop feeds back to the end mirror in the oscillator to ensure that every fourth pulse of the 80 MHz repetition rate output of the oscillator is identical. The slow CEP loop acts on a compressor grating to ensure stability of the amplified pulses. We are able to lock the CEP of the laser at full power to 310mrad rms (measured with 10 ms integration time) for over an hour (Figure 1).

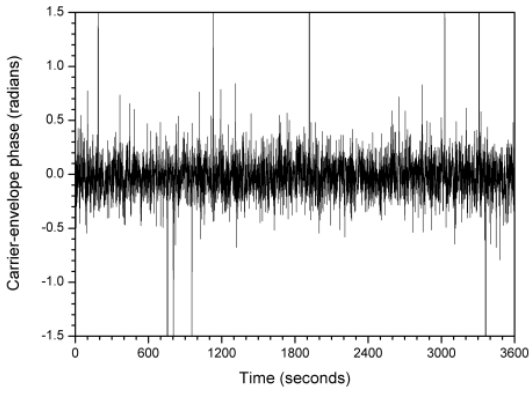

Figure 1. Measured carrier-envelope-phase stability of the Artemis laser system: (a) 310 mrad rms noise over one hour with 13.5 mJ/pulse.

When running the laser with 2mJ/pulse (for compression in the hollow-fibre) we are able to control the phase over a period of five hours (Figure 2) with rms stability of 325 mrad. In this plot, the phase was intentionally ramped so we could acquire data.

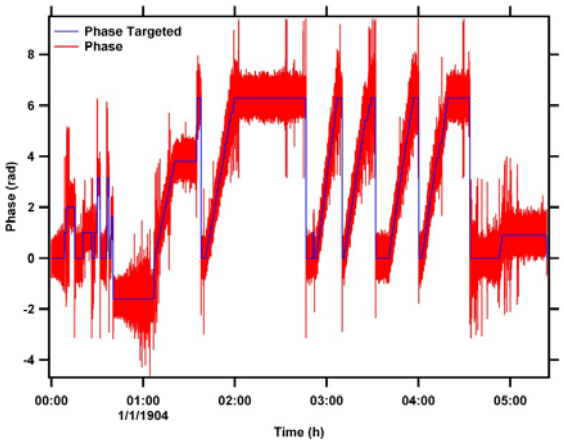

Figure 2. CEP control over five hours with 2mJ/pulse and 325 mrad rms stability. Blue line: programmed target phase. Red line: measured phase.

Few-cycle pulses

Few-cycle laser pulses are produced by splitting off 1 mJ of the laser output and spectrally broadening it in a gas-filled hollow fibre, as previously used in Astra-TA1 [5]. The laser pulses are then recompressed using chirped mirrors. The spectral phase of the few-cycle pulses is measured with SHG-FROG. With 2.2 bar neon pressure in the fibre we obtain 7 fs, 0.5 mJ pulses (Figure 3). This is a substantial improvement on the performance we achieved in Astra-TA1 (which was typically ~ 10 fs). This is due to a combination of changes in focusing into the fibre, improvements in alignment diagnostics, better chirped mirrors and increased bandwidth in the FROG through using a thinner doubling crystal (10 μm BBO).

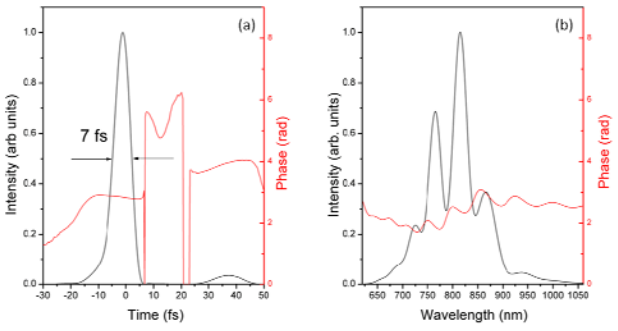

Figure 3. FROG measurement of 7fs, 0.5mJ pulses produced in the hollow fibre system: (a) temporal intensity and phase, (b) spectral intensity and phase. The FROG retrieval error was <0.006.

Conclusions

We have characterized the Artemis few-cycle, carrier-envelope-phase controlled beamline. We measured 7 fs, 0.5 mJ pulses at 1 kHz and have achieved CEP control over a period of 5 hours with rms phase stability of 325 mrad. We have planned further

improvements to the diagnostics and data acquisition with the aim of reducing the pulselength and rms CEP values still further.

Acknowledgements

We thank our technical staff, especially Steve Hook and Toby Strange.

References

1. A. Baltuska et al, “ Attosecond control of electronic processes by intense light fields”, Nature 421, 611 (2003).
2. M. F. Kling et al, “Control of electron localization in molecular dissociation”, Science 312 246 (2006).
3. ICE Turcu et al., “Ultrafast science and development at the Artemis facility”, Proc Proc. SPIE Vol. 7469, 746902 (2010)
4. E. Springate et al., “Artemis: synchronized XUV and laser sources for ultrafast time-resolved science”, CLF Ann Report 2008/9, RAL-TR-2009-025, 221-4 (2009).
5. ICE Turcu et al., “Ten femtosecond laser pulse compression apparatus for Astra target areas”, CLF Ann Report 2004/5, RAL-TR-2005-025, 223-5 (2005).